Monte Carlo study of surface roughness scattering in Si inversion layer with improved matrix element

Won-Jun Cha, Tae-Hun Shim, Jea-Gun Park, et al.

View Online

Export Citation

ARTICLES YOU MAY BE INTERESTED IN

APL Quantum

CALL FOR APPLICANTS
Seeking Editor-in-Chief

AIP Publishing

Monte Carlo study of surface roughness scattering in Si inversion layer with improved matrix element

Won-Jun Cha, Tae-Hun Shim, and Jea-Gun Park[a)]
Department of Electronics and Computer Engineering, Hanyang University, 17 Haengdang-Dong, Seongdong-Gu, Seoul 133-791, Korea

Sang-Dong Yoo
Hynix Semiconductor Inc., San 136-1, Ami-ri, Bubal-eub, Icheon-si, Gyungki-do 467-701, Korea

The electron mobility in the inversion layer of metal oxide semiconductor field-effect transistors was calculated by using a Monte Carlo method. We utilized an improved matrix element for accurately calculating the surface roughness scattering among the many factors determining the electron mobility. The improved matrix element employed different effective electric fields (E_{eff}) for each subband energy level. From the simulation results, we demonstrated that the relative proportion of surface roughness scattering was about three times greater than that of acoustic phonon scattering at an electric field of 1 MV/cm. In particular, the electron mobility curve calculated with the improved matrix element showed better consistency with universal experimental data as compared to a curve calculated with a conventional matrix element. © *2006 American Institute of Physics.*
[DOI: 10.1063/1.2218029]

I. INTRODUCTION

The electron mobility is one of the key factors determining the operating characteristics of metal oxide semiconductor field-effect transistors (MOSFETs). Since the electron mobility degrades as the effective channel length is decreased in scaling down device sizes, electron mobility enhancement is a very active area of research. Many methods and models have been developed for accurately calculating the electron mobility in the silicon (Si) inversion layer of an *n*-type MOSFET.[1–8] The channel junction depth in MOSFETs is scattering down very shallow and decreasing below 20 nm as the channel length of an *n*-MOSFET becomes less than 65 nm. Thus, the importance of surface roughness scattering with respect to other scattering mechanisms is increasing. In addition, all papers published thus far have calculated the surface roughness mobility model without considering electric fields varied by a distance from the surface,[9] by presuming that electrons are localized only in the E_0 subband, where E_0 is the lowest-energy subband in the twofold valleys of the inversion layer. It should be noted, however, that an electron moves farther from the surface through the subbands, in the order of E_0, E_0', and E_1, as shown in Fig. 1, where E_0' is the lowest-energy subband in the fourfold valleys and E_1 is the second lowest-energy subband in the twofold valleys. The surface roughness scattering is proportional to the electron concentration and the surface roughness but inversely proportional to the distance from the Si surface. Since the existing calculation methods have applied a constant electric field throughout the inversion layer, regardless of the energy differences among the subbands, these methods do not account for electric field variation.

Therefore, in this study, we applied an improved matrix element in considering the surface roughness, in which the vertical E_{eff} in the inversion layer depends on the energy value as related to the distance from the surface.

II. THEORETICAL MODELS

The electron transport at room temperature in an inversion layer on a (100) Si surface was calculated by using a single particle Monte Carlo (MC) method. The transverse potential was extracted by using self-consistent solution of Poisson-Schrödinger equation. In addition, three bands in two subband ladders were taken into account, E_0, E_1, and E_2, and E_0', E_1', and E_2', respectively. Since the computational burden increases for full band simulations, we considered nonparabolic electron band model. Three types of scattering
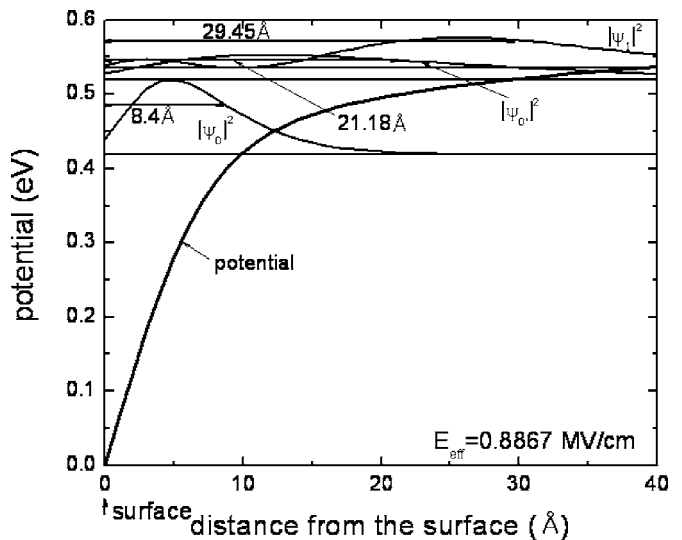

FIG. 1. Potentials, subband energies, and squared subband wave functions for the lowest three subbands, i.e., E_0, E_0', and E_1.

a)Electronic mail: parkjgl@hanyang.ac.kr

TABLE I. Distance of each subband from the Si surface.

Subband	E_0	E_0'	E_1
Distance from Si surface (Å)	8.4	21.18	29.45

mechanisms—acoustic phonon scattering, intervalley phonon scattering, and surface roughness scattering—were considered in calculating the electron mobility.[10] The acoustic phonon scattering and intervalley phonon scattering were calculated using conventional method.[11,12] We assumed no scattering among subbands in the case of acoustic phonon scattering, while for intervalley phonon scattering, we considered two cases of emission and absorption, *f* type and *g* type.[13] Here, *f* type refers to scattering between the same axes, while *g* type refers to scattering between different axes. The *f*-type scattering may occur not only from a low valley to a high valley but also from a high valley to a low valley.[14]

As for the surface roughness scattering, it was calculated as follows. In the range of the quantum limit, a matrix element[15] depending on the potential ΔV produced by surface fluctuation is defined by the following equations:

$$M(\mathbf{k},\mathbf{k}') = \frac{\hbar^2}{2m_3}\Delta_{k-k'}\left|\frac{d\zeta_0}{dz}\right|^2, \qquad (2.1)$$

$$= \Delta_{k-k'}\int dz|\zeta_0|^2\frac{\partial V}{\partial z} \qquad (2.2)$$

$$= \Delta_{k-k'}\left[\frac{4\pi e^2}{\varepsilon_s}\left(\frac{1}{2}N_s + N_{\text{depl}}\right) - \frac{(\varepsilon_s - \varepsilon_{\text{ins}})e}{4\varepsilon_s(\varepsilon_s + \varepsilon_{\text{ins}})}\left\langle\frac{1}{z^2}\right\rangle\right], \qquad (2.3)$$

where N_s is the electron sheet density in the inversion layer, N_{depl} is the charge density of the depletion layer, ε_s is the dielectric constant of Si, ε_{ins} is the dielectric constant of the insulator, and ζ_0 is the wave function of subband energy E_0.

Although Eqs. (2.1) and (2.2) are completely equivalent if we use an exactly self-consistent wave function, Eq. (2.1) indicates scattering due to the localized particles in an inversion layer, while Eq. (2.2) reflects the average scattering for the particles in all inversion layers. Therefore, in the case of varying wave functions, we should employ Eq. (2.2) rather than Eq. (2.1). In Eq. (2.3), the surface roughness scattering is directly proportional to the electron concentration and roughness but inversely proportional to the distance. In most papers about surface roughness mobility model, only the first part of Eq. (2.3) is employed, i.e., E_{eff} is used as a matrix element. In this case, the matrix element does not apply to each subband. Since the surface roughness scattering is inversely proportional to the distance, the probability of electron existence farther from the Si surface increases as a subband rises to a high energy level, as shown in Fig. 1 and Table I.

In addition, the matrix element can be defined by the following equations:

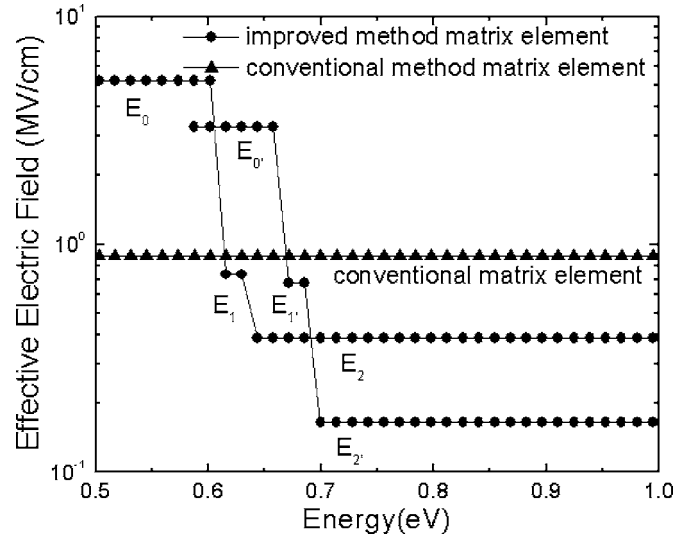$$M^2 = (eV)^2 S(q), \qquad (2.4)$$

FIG. 2. E_{eff} as a function of the subband energy, evaluated using the improved matrix element (cycle) and the conventional matrix element (triangle), considering three subbands in two ladders, i.e., E_0, E_1, and E_2 and E_0', E_1', and E_2', respectively.

$$S(q) = |\Delta(q)|^2, \qquad (2.5)$$

where $S(q)$ is the autocovariance function and $\Delta(q)$ is the Gaussian form of the correlation. In addition, we can consider the autocovariance model of surface roughness scattering proposed by Ando *et al.*,[15]

$$S(q) = \pi\Delta^2 L^2 \exp(-q^2L^2/4), \qquad (2.6)$$

and the model proposed by Goodnick *et al.*,[7]

$$S(q) = \frac{\pi\Delta^2 L^2}{[1 + (q^2L^2/2)]^{3/2}}. \qquad (2.7)$$

In this study, we employed Eq. (2.7) proposed by Goodnick *et al.* and utilized a correlation length $L = 15$ Å and a root-mean-square (rms) roughness amplitude $\Delta = 2$ Å, which is a typical value for a current Si wafer. In addition, we calculated the surface roughness scattering with the following equations:

$$\lambda(\mathbf{k},\mathbf{k}') = \frac{[eE_{\text{eff}}]^2 m_D}{2\pi\hbar^3}\int_0^{2\pi}\frac{S(q)}{\varepsilon(q)^2}d\theta, \qquad (2.8)$$

$$\varepsilon(q) = 1 + \frac{e^2}{2\varepsilon_s\varepsilon_0}\frac{1}{q}\frac{2m_D}{2\pi\hbar^2}F(q), \qquad (2.9)$$

$$F(q) = \int\int|\zeta(z)|^2|\zeta(z')|^2\exp(-q|z-z'|)dzdz', \qquad (2.10)$$

where m_D is the density of state mass, $\varepsilon(q)$ is the dielectric function, and $F(q)$ is the form factor. Equation (2.9) accounts for the screening effect but equals 1 without screening. In this paper, as noted above, we used Eq. (2.2).

III. RESULTS AND DISCUSSION

Figure 2 shows the E_{eff} as a function of the subband energy. The triangles represent the simulated results obtained by utilizing a constant effective field regardless of the sub-

FIG. 4. Relative electron occupancy in each subband as a function of the effective electric field, evaluated using a single particle MC method and employed self-consistent solution of Poisson-Schrödinger equation.
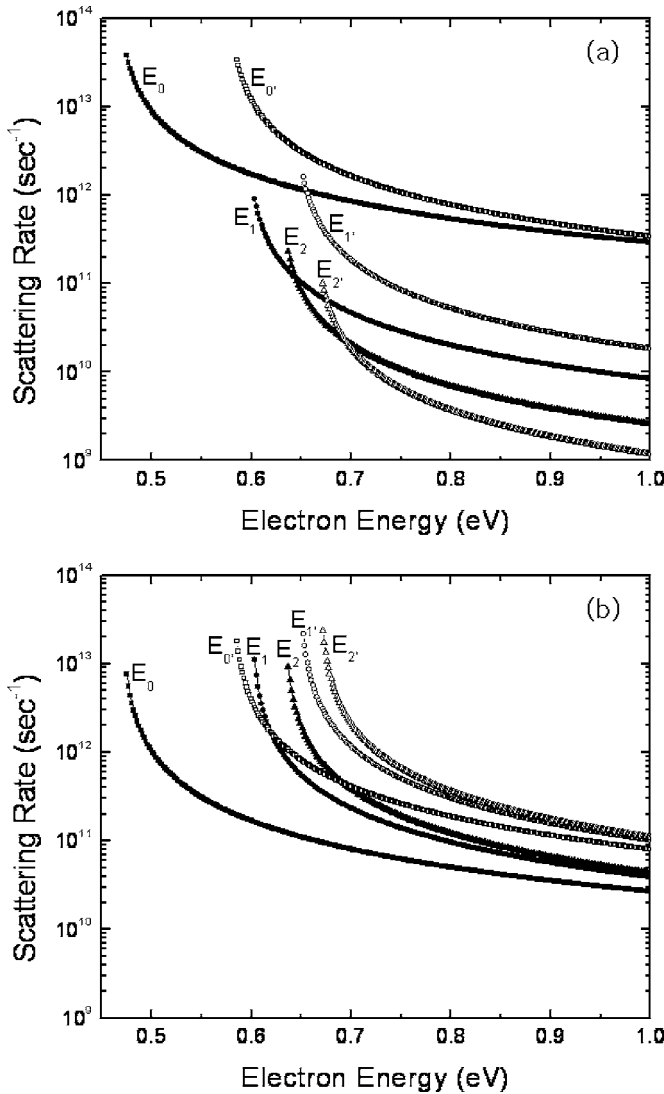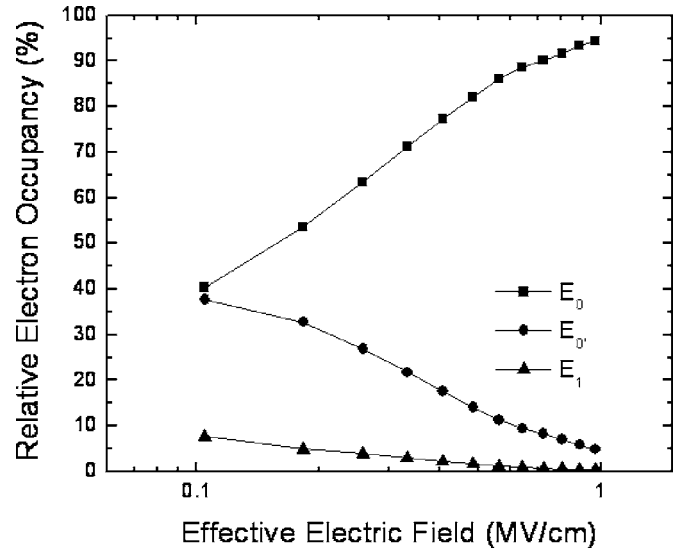

FIG. 3. (a) Surface roughness scattering rate in three subbands of two ladders with the improved matrix element, showing the onsets of scattering for each subband begin with a different value. (b) Surface roughness scattering rate in three subbands of two ladders with the conventional matrix element, showing the onset of scattering for all subbands start at almost the same level of value.

band, while the circles represent the simulated results obtained by using a different E_{eff} for each subband. The circles clearly show how the E_{eff} depends on the energy difference for each subband, thus indicating more accurate simulation of the surface roughness scattering.

Figures 3(a) and 3(b) show the surface roughness scattering rate, as simulated with the improved matrix element and the conventional matrix element, respectively. The onsets of scattering in Fig. 3(a) begin with a different scattering rate value for each subband, while the onsets in Fig. 3(b) begin with almost the same value for each subband. This difference occurred because for the simulation results shown in Fig. 3(a), the improved matrix element was applied with a different E_{eff} for each subband. In addition, the results indicate that with the improved matrix element, the scattering rate of the lowest subband, with energy E_0, is the highest among all the subbands, because this subband is the closest to the Si surface. In particular, the results show different

scattering rates for each subband. Note that the portion of electron occupancy in the lowest subband, with energy E_0, rises as the E_{eff} increases to a high value. Thus, the improved method can reflect the surface roughness scattering more explicitly than the conventional method.[16]

Figure 4 shows the relative electron occupancy in each subband as a function of the E_{eff}, indicating that the relative electron occupancy in the E_0 subband increases considerably with the E_{eff}. This illustrates why different E_{eff} for each subband should be applied. The figure also indicates that the surface roughness scattering, which is inversely proportional to the distance, is influenced mostly by the E_0 subband as the E_{eff} increases, since the E_0 subband is the closest to the Si surface.

Figures 5(a) and 5(b) show the relative scattering among the acoustic phonon scattering, intervalley phonon scattering, and surface roughness scattering, as obtained with the improved matrix element and the conventional matrix element, respectively. The results shown in Fig. 5(a) indicate that the relative portion of surface roughness scattering increases dramatically at an E_{eff} of more than 0.5 MV/cm. In particular, it is about three times greater than the acoustic phonon scattering at an E_{eff} of 1.0 MV/cm. Otherwise, the relative portion of surface roughness scattering shown in Fig. 5(b) increases moderately and remains much smaller than that shown in Fig. 5(a), where it is about 1.15 times greater than the acoustic phonon scattering at 1.0 MV/cm. From these results, it is evident that the improved method can more accurately simulate the surface roughness scattering in a high range of the E_{eff}, as compared to the conventional method.

Finally, Fig. 6 shows the electron mobility curves obtained as a function of the E_{eff} in this work and other works. The comparison indicates good agreement throughout the range of E_{eff} between an experimental universal curve and the simulated curve obtained with the improved method. In particular, the slope of the electron mobility for the improved method at greater than 0.5 MV/cm is strongly consistent
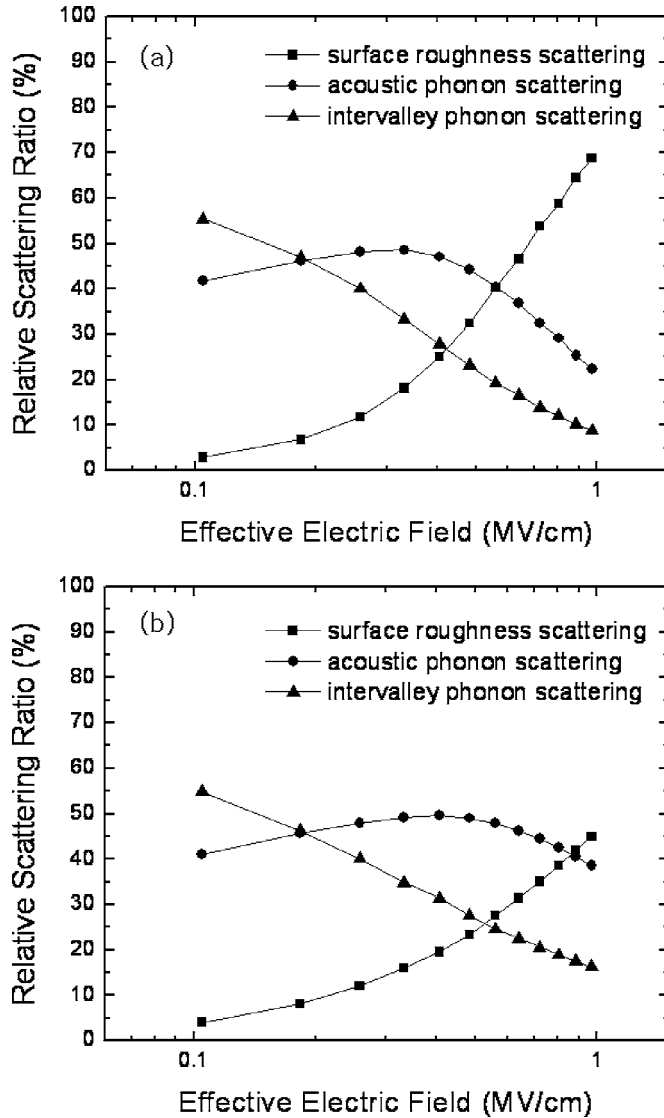
FIG. 5. Relative scattering ratios of acoustic phonon scattering, intervalley phonon scattering, and surface roughness scattering, (a) with the improved matrix element and (b) with the conventional matrix element, showing surface roughness scattering in (a) is most dominant among three scattering mechanisms in high range of electric fields, while surface roughness scattering rate in (b) is suppressed in high range of electric fields.

with the slope of the universal effective electron mobility, as well as with that for simulated results taken from Ref. 17, which do not account for the screening effect. Moreover, the figure shows that the slope for the improved method is a little bit lower in the range of E_{eff} above 0.5 MV/cm as compared to the universal electron mobility curve. Otherwise, the slope for the conventional method is higher in this same range. In addition, the figure indicates the stronger E_{eff} dependencies of both simulated curves as compared with the universal curve. This discrepancy can be explained in terms of the screening effect of electrons at a higher sheet density. Recall here that we did not consider the screening effect in our simulation. Therefore, we conclude that the improved method produced results more consistent with the universal experimental mobility curve, as compared to the conventional method. In particular, the surface roughness scattering
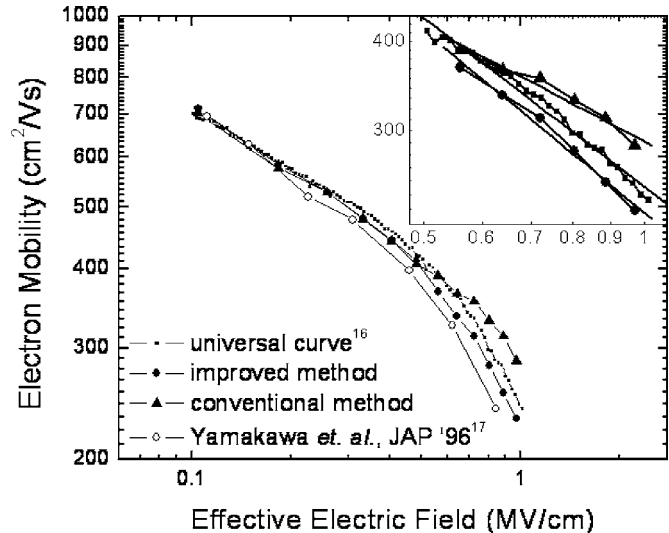

FIG. 6. Comparison of electron mobility curves simulated in this work and other works.

obtained with the improved matrix element appeared much more explicitly in the higher range of E_{eff}, as compared with the conventional matrix element.

IV. CONCLUSION

The relative surface roughness scattering with respect to two other scattering mechanisms, where all three mechanisms determine the electron mobility, was studied using a MC method. In particular, the surface roughness scattering obtained with an improved matrix element, which considered a different E_{eff} for each subband energy level, was compared with that obtained with a conventional matrix element applying a constant E_{eff} for each subband energy level. Form the results, we found that the improved matrix element more accurately reflected the locations and movements of electrons, and we clearly demonstrated that the relative proportion of surface roughness scattering dominantly increased in the range of E_{eff} above 0.5 MV/cm as compared with the acoustic and intervalley phonon scattering. In particular, we showed that at an electric field of 1 MV/cm, the relative surface roughness scattering increased to about three times that obtained with the conventional method. In addition, the electron mobility curve simulated with the improved matrix element exhibited a slope more consistent with that of a universal experimental electron mobility curve in the range above 0.5 MV/cm, as compared to the conventional matrix element.

ACKNOWLEDGMENTS

[1] H. R. Huff, G. A. Brown, L. A. Larson, and W. Murto, ECS PV 2001–9, Vol. 263, p. 9.
[2] M. Shirahata and C. Hamaguchi, Jpn. J. Appl. Phys., Part 1 **25**, 1040 (1986).

[3]J. A. Cooper and D. F. Nelson, J. Appl. Phys. **54**, 1445 (1983).

[4]A. Hartstein, T. H. Ning, and A. B. Fowler, Surf. Sci. **58**, 178 (1976).

[5]K. Masaki, C. Hamaguchi, K. Taniguchi, and M. Iwase, Jpn. J. Appl. Phys., Part 1 **28**, 1856 (1989).

[6]W. K. Masaki, C. Hamaguchi, K. Taniguchi, and M. Iwase, Jpn. J. Appl. Phys., Part 1 **30**, 2739 (1991).

[7]S. M. Goodnick, D. K. Ferry, C. W. Wilmsen, Z. Liliental, D. Fathy, and O. L. Krivanek, Phys. Rev. B **32**, 8171 (1985).

[8]T. Yoshinobu, A. Iwamoto, and H. Iwasaki, Jpn. J. Appl. Phys., Part 1 **26**, 1447 (1987).

[9]Y. Matsumoto, Jpn. J. Appl. Phys., Suppl. **2**, 367 (1974).

[10]C. Jacoboni and L. Reggiani, Rev. Mod. Phys. **55**, 645 (1983).

[11]J. P. Polonovski and K. Tomizawa, Jpn. J. Appl. Phys., Part 1 **24**, 1611 (1985).

[12]P. J. Price, Ann. Phys. (N.Y.) **133**, 217 (1981).

[13]S. Imanaga and Y. Hayafuji, J. Appl. Phys. **70**, 1522 (1991).

[14]S. Takagi, J. L. Hoyt, J. J. Welse, and J. F. Gibbons, J. Appl. Phys. **80**, 1567 (1996).

[15]T. Ando, A. B. Fowler, and F. Stern, Rev. Mod. Phys. **54**, 437 (1982).

[16]S. Takagi, A. Toriumi, M. Iwase, and H. Tango, IEEE Trans. Electron Devices **41**, 2357 (1994).

[17]S. Yamakawa, H. Ueno, K. Taniguchi, and C. Hamaguchi, J. Appl. Phys. **79**, 911 (1996).